POLITECNICO DI TORINO
Repository ISTITUZIONALE

Numerical Modeling of the Emission Characteristics of Semiconductor Quantum Dash Materials for Lasers and Optical Amplifiers

(Article begins on next page)

05 August 2020

Numerical Modeling of the Emission Characteristics of Semiconductor Quantum Dash Materials for Lasers and Optical Amplifiers

Mariangela Gioannini

Abstract—This paper deals with the simulation of the emission characteristics of self-assembled semiconductor quantum dash (QDash) active materials, characterized by high length-to-width and width-to-height ratios of the dash size and by a wide spreading of the dash dimensions. This significant size fluctuation requires to compute numerically the corresponding energy distribution of the electron and hole confined states. Furthermore, due to the long dash length, it is necessary to take into account the many longitudinal confined states that contribute to the emission spectrum. To implement a model that does not require excessive computation time, some simplifying assumptions have been introduced and validated numerically. Starting from good knowledge of the dash size, material composition, and optical waveguide dimensions, we have been able to simulate the amplified spontaneous emission and gain spectra of a quantum dash semiconductor optical amplifier with a good quantitative agreement with the measured data. As an application example, the model is used to predict the gain properties of different QDash ensembles having various size distributions.

Index Terms—Modeling, optical gain, quantum dash (QDash), quantum-dot lasers, self-assembled.

I. INTRODUCTION

IN THE LAST decade, a great deal of research on semiconductor materials has focused on the theoretical and experimental study of self-assembled semiconductor nanostructures [1] and has shown the superior electronic and optoelectronic properties obtained by the three-dimensional (3-D) confinement of carriers [2], [3]. The carrier confinement in a few bounded states—the ground state and the excited state—in quantum dots (QDs) is obtained by the very small dot size, below or around the exciton Bohr radius. Using a QD ensemble as gain medium for semiconductor lasers and optical amplifiers, significant improvements with respect to the quantum well and wire cases have been obtained in the threshold current, differential gain, linewidth enhancement factor, chirp, and high-speed dynamics [4]–[6].

Very recently, new elongated nanostructures have also been grown with quantum dash (QDash) [7], [8] or rod shapes [9]. QDashes appear at scanning and transmission electron microscopy images [8] with a cross section of the same size of QDs (about 2–3 nm × 10–20 nm) and a length of hundreds of nanometers (100–200 nm). Thanks to their elongated form, QDashes have a high number of longitudinal confined states that can be filled at a fairly low pump current density. Together with size fluctuations of the transversal cross section, this produces a very wide gain spectrum [10]–[12]. The advantageous properties derived from the zero-dimensionality [e.g., low threshold current and linewidth enhancement factor (LEF)] are maintained as well [12]. QDash material is thus promising for a variety of optoelectronic devices that benefit from broad optical gain spectra. For example, the QDash material finds application as an active medium of semiconductor optical amplifiers (SOAs) [13] and single-mode lasers [14], which can cover all the necessary wavelengths (1400–1650 nm) of future multiwavelength optical transmission systems [11]. QDash lasers in an external-cavity configuration have also been used to obtain a very wide tuning range of about 150 nm [15].

QDashes are grown by self-assembled epitaxial growth with high width-to thickness and length-to-width ratios. This growth technique gives also a wide stochastic size distribution that produces an energy spreading of the various confined levels, each contributing to the inhomogeneous broadening of the gain spectrum. The result is a continuous inhomogeneously broadened emission spectrum extended over a wide wavelength range. The control of the dash size and its spreading is thus fundamental to engineer the gain properties of the QDash material and numerical models that allow to quantitatively predict the gain, and spontaneous emission characteristics can be useful to give directions to select the proper growth parameters.

The effect of size fluctuations on the gain and photoluminescence spectra of QD materials has been theoretically analyzed in [16]–[18]. Compared to a QD ensemble, where only a few electron and hole states contribute to gain [18], [19], QDashes grown on InP [8] have usually one or two quantized states with respect to the transversal cross section [20] and a high maximum quantization order in the longitudinal direction due to the long dash length. This peculiar characteristic of InAs–InP QDashes increase, with respect to QD, the complication in the development of a reliable numerical model.

In the literature, the consequence of the dot size fluctuation is usually modeled introducing a reduced density of states with a Gaussian distribution [19], [21], whose full-width at half-maximum (FWHM) is analytically calculated assuming a linear variation of the energy levels [19], but this assumption is valid only in the case of narrow size fluctuations. To our knowledge, a detailed theoretical analysis of the effect of size fluctuations has been presented only in [18], but the investigation was limited

to the QD case and only the ground state emission was considered. In other work [22], the FWHM is extracted by the measured spontaneous emission spectra, but this is possible only when the different contributions from the ground state and the excited states can be clearly separated.

In QDash materials, the confined energy levels have a nonlinear variation due to the high length-to-width and width-to-thickness ratios and due to the simultaneous fluctuation of the three dimensions of the dashes of the ensemble. As a result, the inhomogeneous broadening functions of the states can significantly differ from a Gaussian shape. Moreover, the width of the inhomogeneous broadening can not be found from experiments, because many levels of different order contribute altogether to the emission spectrum, making it impossible to separate each contribution. As a consequence, to understand the influence of the inhomogeneous linewidth on the emission characteristics, it is necessary to calculate numerically the inhomogeneous broadening functions for any given size distribution.

Another feature of the InAs–InP QDash system is the difference between the InAs hole effective mass and the electron effective mass. This can give a higher number of energy levels in valence band (VB) compared to the conduction band (CB) and can cause the thermal smearing of the hole population among many states, limiting the gain performance [23].

The knowledge of the energy level position in CB and VB varying the dash size is thus necessary to quantify the inhomogeneous broadening effect on the spectral emission characteristics—e.g., gain and amplified spontaneous emission (ASE)—and calculate the carrier distribution among the confined states.

In this paper, we present a numerical model for the calculation of the gain and ASE spectra at different pump rates of a realistic InAs–InP QDash SOA [13] realized with the QDash material presented in [8]. The paper is organized as follows. In Section II, we first present and validate the numerical method and the approximations introduced to calculate the CB and VB confined states in the QD, and then we present the numerical model for the calculation of the inhomogeneous broadening functions and the spectral emission characteristics. In Section III, we validate our model through a quantitative comparison with experimental results and, as an example of application, we show how the average dash size and its fluctuation influence the gain spectrum characteristics. Finally, in Section IV, we draw the conclusions.

II. NUMERICAL MODEL OF EMISSION CHARACTERISTICS

The numerical calculation of the emission characteristics of a QDash ensemble proceeds in two steps. In the first step, to correctly account for any given size distribution, the model calculates all of the CB and VB confined state energy levels, the recombination wavelengths, and the overlap integrals between the CB and VB wave functions for all of the QDash sizes present in the ensemble. In the second step, all of these data are numerically processed to obtain the inhomogeneous broadening functions used to calculate the gain and spontaneous emission spectra at different carrier injections.

A. Calculation of Electronic States

For the calculation of electronic states of QD, several numerical schemes have been presented in the literature, even with high degrees of sophistication, including the strain effects, the Coulomb interaction among charged confined carriers, and considering various dot shapes [24], [25]. All of these models are very accurate but, as a tradeoff, they require a long computation time. In the case of QDash modeling, to account for the wide size spreading, the calculation of the confined states in CB and VB has to be repeated several times for each dash size of the ensemble, and this would lead to an unacceptable computation time. To get reliable results with a reasonable computational complexity and short simulation times, we have introduced some approximations in the dash shape, in the modeling of strain effects, and in the solution of the Schrödinger equations.

In our model, the confined states of a single dash have been obtained calculating the eigenvalues of the single-particle Schrödinger equation in the effective mass approximation, considering finite barriers and different effective masses for the dash and barrier materials. The Schrödinger equation for the electrons is given by

$$-\frac{\hbar^2}{2}\nabla\frac{1}{m_e^*}\cdot\nabla\psi_e(x,y,z)+\Delta E_{\mathrm{CB}}(x,y,z)\psi_e(x,y,z)$$
$$=E_{\mathrm{CB}}\psi_e(x,y,z) \quad (1)$$

where $\Delta E_{\mathrm{CB}}(x,y,z)$ is the CB confinement potential, E_{CB} is the confined state energy, $\psi_E(x,y,z)$ is the corresponding wave function, and m_e^* is the electron effective mass.

The Schrödinger equation for the holes in VB is

$$-\frac{\hbar^2}{2}\left[\nabla_{xz}\frac{1}{m_{h,\|}^*}\cdot\nabla_{xz}+\nabla_y\frac{1}{m_{h,\perp}^*}\cdot\nabla_y\right]\psi_h(x,y,z)$$
$$+\Delta E_{VB}(x,y,z)\psi_h(x,y,z)=E_{\mathrm{VB}}\psi_h(x,y,z) \quad (2)$$

where ΔE_{VB} is the VB confinement potential, ∇_{xz} and ∇_y are the gradient in the parallel and perpendicular plane, respectively (see Fig. 1), and $m_{h,\|}^*$ and $m_{h,\perp}^*$ are the hole effective masses in the perpendicular and parallel direction and account for the modification induced by the strain [25]. In our model, we have neglected the coupling with the light-hole and split-off bands, because in the presence of compressive strain—as for the InAs dash we consider—these two bands are split far away from the VB edge and play a negligible role [26].

An SEM image [8] of the QDash ensemble under investigation is presented in Fig. 1(a); the shape of the single dash [circled area in Fig. 1(a)] has been approximated with an elongated semiparabolic geometry as shown in Fig. 1(b). On this geometry, the solution of the Schrödinger equation has been carried on with the 3-D finite element method (FEM), but the resulting computation time was very long. On the contrary, the solution carried out using a factorization procedure, similar to the equivalent refractive index (ERI) method used in integrated optics [27], has proved to be much faster. However, the ERI-like method is really efficient if applied to a box structure, because we can solve the single-particle eigenvalue equation only one time in each direction. Furthermore, the method is a good approximation when,
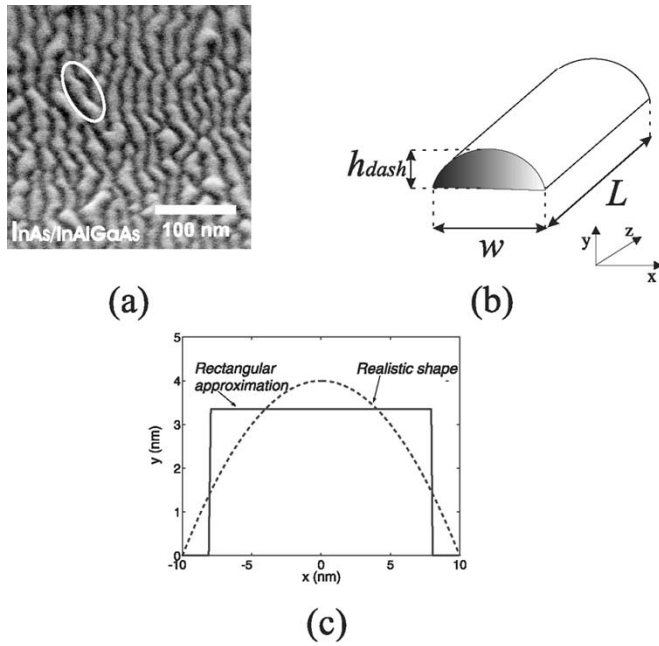
Fig. 1. (a) SEM image of the InAs QDash ensemble grown over a InAlGaAs substrate [8]. (b) Schematic shape of a single dash. (c) Rectangular approximation of the transversal cross section.

as in the dash case, the box thickness is much smaller than the box width, which in turn is smaller than the length. The semi-parabolic cross section [the xy plane in Fig. 1(b)] has thus been approximated with an equivalent rectangular shape as shown in Fig. 1(c). The equivalent rectangle has been chosen to have the same area of the transversal cross section and to satisfy a minimum distance criterion from the parabolic function.

The ERI method factorizes the Schrödinger equation in three directions: the eigenvalues of the particle in the well in the y direction give first the energies E_m. Then the states E_n are obtained from the factorization in the x direction with a well energy barrier reduced by E_m. The same procedure is repeated to find the states E_k due to confinement in the longitudinal direction. The energies of the dash confined states are thus $E_{mnk} = E_m + E_n + E_k$. The resulting confined state wave functions also have simple expressions and their overlap integrals can be easily calculated analytically [27]. To accurately model the dash inner and outer mass discontinuity, in our ERI-like method the particle effective mass in each factorization step has been chosen to be equal to a mass that is the weighted average of the dash and barrier mass [28]. The weight coefficient is given by the confinement factor in the dash of the wave function calculated in the prior factorization step.

In order to quantify the errors introduced by the rectangular approximation and by the numerical factorization, we have compared the transversal energy levels (eigenvalues of the Schrodinger equation in the xy plane), obtained applying the two-dimensional (2-D) FEM analysis with those calculated using the ERI-like method to the corresponding equivalent rectangular structures. As an example, we report in Fig. 2(a) the CB energy levels versus the thickness of an InAs dash embedded in InAlGaAs; for this simulation the dash width is $w = 20$ nm. In the figure, the circles correspond to the eigenvalues calculated for semiparabolic dashes, whereas the

squares are the eigenvalues of the equivalent rectangle. The dashed lines are the fitting with the function proposed in [18]. For the confined state E_{00}, the numerical error in the energy level ranges between 3 ($h = 1.4$ nm) and 7.8 meV ($h = 7$ nm). For the E_{01} state, the error is between -12.4 ($h = 1.4$ nm) and -7 meV ($h = 7$ nm). To quantify the impact of these numerical errors on the emission characteristics, we have compared the FWHM of the inhomogeneous linewidth of the CB density of states obtained by the energy distributions that result from the FEM and ERI-like method. Several QDash ensembles of various average thicknesses (μ_h) and thickness spreading (σ_h) have been considered. The results, reported in Fig. 2(b), show that the box approximation introduces negligible errors in the inhomogeneous broadening (less than 2% for $\mu_h = 2.8$ nm and less than 4.5% for $\mu_h = 5.6$ nm). We can thus conclude that the rectangular cross-section assumption introduces only a shift in the calculated eigenvalues [Fig. 2(a)] toward higher energies for the E_{00} state and toward lower energies for the E_{01} state. Nevertheless, the inhomogeneous broadening linewidth can be obtained with a good accuracy [Fig. 2(b)]. In fact, since the purpose of this study is to find the relation between the dash size spreading and the emission characteristics, we are not concerned about obtaining a very accurate knowledge of the energy values of the confined states, but rather in the effect produced by their wide fluctuations.

The error introduced by the longitudinal factorization [the z direction in Fig. 1(a)] can be estimated from the results in Fig. 3. An InAs box ($h = 1.8$ nm, $w = 17.3$ nm, $L = 80$ nm) embedded in InAlGaAs has been considered and the energy levels have been calculated by the FemLab 3-D solver and the ERI-like method. The results are reported versus the longitudinal quantum index k in Fig. 3. The figure shows that the numerical error due to factorization is practically null for low k values (0 and 1) and increases with $k \geq 2$. However, these numerical errors for high k are negligible. We have indeed observed that the energy levels with high k experience energy variations, due to length fluctuations, much wider than the factorization numerical error.

This particle-in-a-box approach has been used to analyze the effect of the dash thickness, width, and length fluctuations on the emission characteristics of a self-assembled QDash material. As an example, we plot in Fig. 4(a) the recombination wavelengths of an ensemble with length variation from 20 to 150 nm at 10-nm steps. The dash transversal cross section is fixed to 2.2 nm $\times$ 16 nm. In this simulation, we assume that only the recombination between CB and VB energy levels with the same quantum index are really efficient. The symbols on each row of Fig. 4(a) represent recombinations with the same quantum index mnk occurring in QDashes of different length (the length increases toward longer wavelengths). This figure shows that all recombinations with $k = 0$ index (000 and 010) all squeeze into a narrow wavelength range (e.g., 1650–1700 nm for 000), whereas recombinations with $k \geq 1$ values are nonuniformly spread over a wider wavelength range (e.g., 1450–1650 nm for 004). This example demonstrates that the recombination wavelength does not change linearly for a linear length variation and that the energy level spreading is significantly dependent on the confined state quantum index.
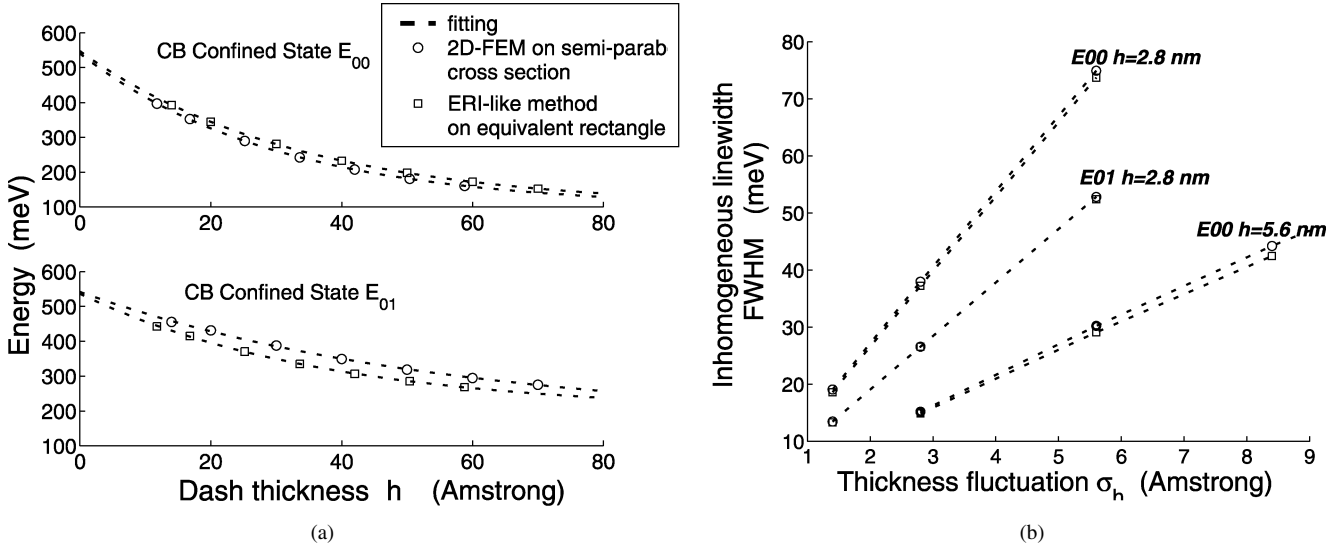
Fig. 2. (a) Eigenvalues of the CB Schrödinger equation in the transversal plane versus the dash thickness calculated with the 2-D FEM method (circles) and the ERI-like method (squares) on the equivalent rectangle. The dashed line is the fitting with the function proposed in [18]. (b) The resulting FWHM of the inhomogeneous broadening versus the standard deviation of the thickness spreading σ_h around the average values $h = 2.8$ nm and $h = 5.6$ nm. For $h = 5.6$ nm, the FWHM of the state 01 is not shown because it practically overlaps with the 00 one.
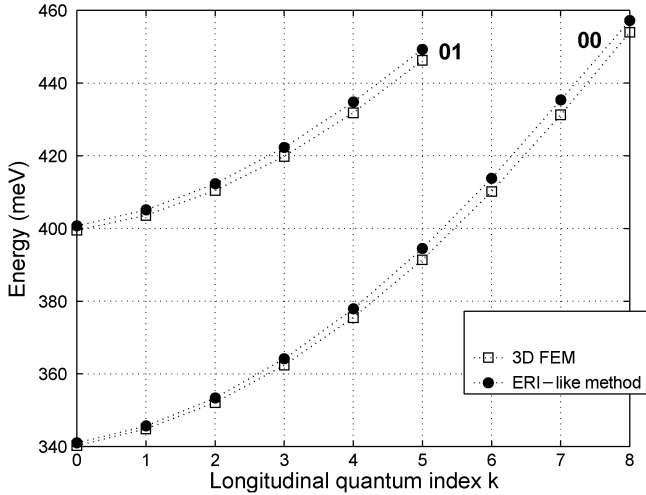

Fig. 3. CB energy levels of a box dash ($h = 1.8$ nm, $w = 17.3$ nm, $L = 80$ nm) calculated with the 3-D FEM (square symbols) and the ERI-like (dot symbols) method.

To understand how the confined state wave function impacts the recombination efficiency, we plot in Fig. 4(b) the values of the overlap integrals calculated at the wavelengths of Fig. 4(a). We observe that the overlap integrals depend only on the wavelength and on the transversal index mn, whereas they are practically independent of the k index.

Similar figures can be obtained in the case of width variations. In the case of thickness fluctuations, the energy levels spread more uniformly but the extension of the wavelength range is still dependent on the recombination quantum index.

B. Calculation of the Emission Spectra Characteristics

According to the density matrix model [1], [29], the gain and the spontaneous emission of a zero-dimensional active material is given by the sum of the contributions of each recombination between CB and VB confined states. Considering, for simplicity, only the recombination between CB and VB energy states with the same quantum index, $\varepsilon_{mnk,\mathrm{CB}}$ and $\varepsilon_{mnk,\mathrm{VB}}$, the contribution to the material gain and to the spontaneous emission rate, $g_{mnk}(\hbar\omega)$ and $R_{\mathrm{sp}_{mnk}}(\hbar\omega)$ (in $\mathrm{cm}^{-2}\cdot eV^{-1}\cdot\mathrm{s}^{-1}$) are given by [1]

$$g_{mnk}(\hbar\omega) = \frac{C_g}{\hbar\omega} \cdot \int M_b^2 \cdot \frac{2}{V_0} L(\hbar\omega - \varepsilon)$$

$$\cdot [f_n(\varepsilon_{mnk,\mathrm{CB}}) + f_p(\varepsilon_{mnk,\mathrm{VB}}) - 1] \cdot P_{mnk}(\varepsilon) \cdot d\varepsilon \qquad (3)$$

and

$$R_{\mathrm{sp}_{mnk}}(\hbar\omega) = \Gamma_{xz} \cdot h_{ave} \frac{1}{\hbar\omega} \cdot \frac{\pi e^2 \hbar}{n_r^2 \varepsilon_0 m_0^2} \cdot \int M_b^2 \cdot \frac{2}{V_0}$$

$$\cdot L(\hbar\omega - \varepsilon) \cdot [f_n(\varepsilon_{mnk,\mathrm{CB}}) \cdot f_p(\varepsilon_{mnk,\mathrm{VB}})]$$

$$\cdot \rho_{\mathrm{opt}}(\hbar\omega) \cdot P_{mnk}(\varepsilon) \cdot d\varepsilon \qquad (4)$$

where $\hbar\omega$ is the recombination energy and $\varepsilon = \varepsilon_{mnk,\mathrm{CB}} + \varepsilon_{mnk,\mathrm{VB}} + E_g$, $C_g = \pi\hbar e^2/(m_0^2 \varepsilon_0 c n_r)$ where e is the electron charge, m_0 is the free-electron mass, ε_0 is the dielectric permittivity, c is the light velocity, and n_r is the refractive index, M_b^2 is the transition matrix element given by the product of the interband matrix element and the overlap integral (I_{mnk}^2) between the envelope functions of the electron and hole involved in the transition [21]

$$M_b^2 = \frac{m_0^2}{12 m_e^*} \cdot \frac{E_g(E_g + \Delta)}{E_g + \frac{2}{3}\Delta} \cdot I_{mnk}^2$$

where m_e^* is the electron effective mass, E_g is the energy gap, and Δ is the split-off band, V_0 is the volume of the dash that participates to the emission, $L(\hbar\omega - \varepsilon)$ is a Lorentzian function centered in $\hbar\omega$ with FWHM equal to $2\Delta\gamma$ that takes into
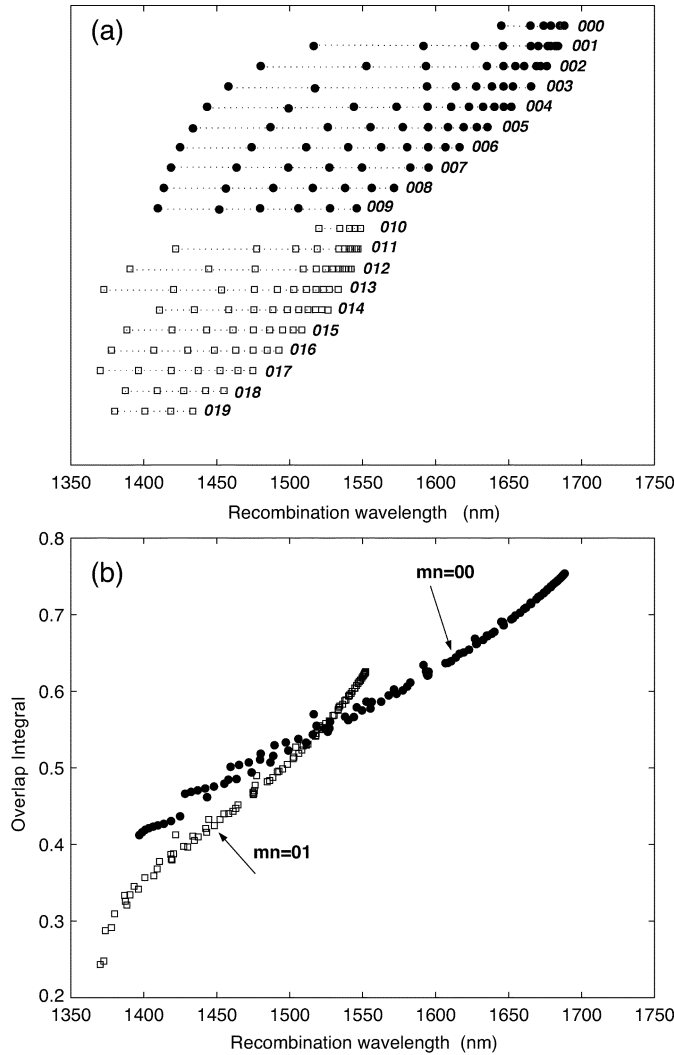
Fig. 4. (a) Recombination wavelengths and (b) corresponding overlap integrals calculated for box dashes with a cross section of 2.2 nm × 16 nm and length varying from 20 to 150 nm with 10-nm steps. The dot and square symbols are for 00 and 01 transversal recombination index, respectively. The symbols on each row in (a) correspond to different dash lengths.

account homogeneous broadening due to the polarization dephasing [21]

$$L(\hbar\omega - \varepsilon) = \frac{1}{\pi} \cdot \frac{\Delta\gamma}{(\hbar\omega - \varepsilon)^2 + (\Delta\gamma)^2}.$$

$f_n(\varepsilon_{mnk,\mathrm{CB}})$ and $f_p(\varepsilon_{mnk,\mathrm{VB}})$ are the electron and hole occupation probabilities of the discrete states $\varepsilon_{mnk,\mathrm{CB}}$ and $\varepsilon_{mnk,\mathrm{VB}}$. Γ_{xz} is the in-plane (plane xz in Fig. 1) filling factor of the ensemble, and h_{ave} is the average QD thickness. $\rho_{\mathrm{opt}}(\hbar\omega) = (1/\pi^2) \cdot (n_r^3(\hbar\omega)^2/(\hbar c)^3)$ is the density of the optical modes [28].

In (3) and (4), the term $P_{mnk}(\varepsilon)$ is a probability density function (pdf) and the term $P_{mnk}(\varepsilon)d\varepsilon$ corresponds to the probability of having a recombination between a CB and VB state with quantum index mnk and recombination energy in the range $[\varepsilon - d\varepsilon/2, \varepsilon + d\varepsilon/2]$, where $d\varepsilon$ is an infinitesimal interval around ε. This term takes into account the size fluctuation of the dashes [21] and represents the inhomogeneous broadening contribution to the emission spectrum. Compared to [19]

and [21], where the inhomogeneous broadening function is written as a Gaussian distribution, in our model $P_{mnk}(\varepsilon)$ is numerically determined starting from the distribution of the QDash dimension fluctuations.

The total material gain $g_{\mathrm{mat}}(\hbar\omega)$ and the total spontaneous emission rate $R_{\mathrm{spon}}(\hbar\omega)$ are obtained by the sum of all the mnk contributions.

To simulate the emission characteristics, through (3) and (4), we first numerically calculate all the confined state energy levels of the ensemble ($\varepsilon_{mnk,\mathrm{CB}}$ and $\varepsilon_{mnk,\mathrm{CV}}$) and the overlap integrals I_{mnk} with the ERI-like method presented in Section II-A. All these data are then postprocessed to numerically determine the inhomogeneous broadening function $P_{mnk}(\varepsilon)$ and the occupation probabilities f_n and f_p.

1) Calculation of the Inhomogeneous Broadening Functions $P_{mnk}(\varepsilon)$: The dash-size fluctuation is modeled assuming that each QDash dimension fluctuates with an independent Gaussian distribution, with average value $\mu_{h,w,L}$ and standard deviation $\sigma_{h,w,L}$. Considering fluctuations in the growth, lateral, and longitudinal directions in the ranges $[h_{min}, h_{max}]$, $[w_{min}, w_{max}]$, and $[L_{min}, L_{max}]$, respectively, the simulator calculates all of the recombination energies varying simultaneously the QDash thickness, width, and length with discretization steps Δh, Δw, and ΔL. Among the calculated values it determines the recombination energies between the CB and VB states with quantum index mnk falling in the range $[\varepsilon - d\varepsilon/2, \varepsilon + d\varepsilon/2]$ and the corresponding dash size (h_i, w_i, L_i). The term $P_{mnk}(\varepsilon) \cdot d\varepsilon$ is numerically calculated as

$$P_{mnk}(\varepsilon) \cdot d\varepsilon = \Sigma_i p_{h_i} \cdot p_{w_i} \cdot p_{L_i} \qquad (5)$$

where p_{h_i}, p_{w_i}, and p_{L_i} are respectively the probabilities of having the QDash thickness, width, and length in the range $[h_i - \Delta h/2, h_i + \Delta h/2]$, $[w_i - \Delta w/2, w_i + \Delta w/2]$, and $[L_i - \Delta L/2, L_i + \Delta L/2]$. For a Gaussian distribution of the size fluctuations, these probabilities are easily obtained by the error function erf [31].

2) Calculation of the Occupation Probabilities $f_n(\varepsilon_{mnk,\mathrm{CB}})$ and $f_p(\varepsilon_{mnk,\mathrm{VB}})$: To calculate accurately the occupation probabilities of each confined state in CB and VB, a multilevel rate-equation model should be implemented [32] including the particle scattering among levels due to the interaction with phonons, the radiative and nonradiative recombinations, and the coupling, through the wetting layer (WL), among dash populations of different sizes [33]. However, at room temperatures, the electron and hole populations equilibrate in each layer and with the WL [32], [34], thanks to the higher scattering rates between the QDash electronic states compared to the spontaneous emission rate. As a consequence, we can define the occupation probabilities in the confined and wetting layer states through a Fermi distribution that is determined by the electron and hole quasi-Fermi levels E_{Fe} and E_{Fh}. We assume that the values of E_{Fe} and E_{Fh} are constant for all of the dashes of the ensemble (no size dependence) and for the WL (thermal equilibrium with the carrier population in the dashes). E_{Fe} and E_{Fh} are set applying the charge neutrality condition to a unit area of the QDash ensemble [23] as follows:

$$N_s \cdot n_{\mathrm{QD}} + d_{WL} \cdot n_{\mathrm{WL}} = N_s \cdot p_{\mathrm{QD}} + d_{\mathrm{WL}} \cdot p_{\mathrm{WL}} \qquad (6)$$

where N_s is the density of dash per unit area and d_{WL} is the depth of the WL. In (6), n_{QD} and p_{QD} are the numbers of electrons and holes in the average dash of the ensemble as follows:

$$n, p_{\mathrm{QD}} = \sum_{mnk} \frac{1}{1 + e^{\frac{\overline{\varepsilon}_{mnk_{\mathrm{BC,BV}}} - E_{Fe,h}}{KT}}}$$

where the sum is over all the CB or VB confined states of the average dash ($\overline{\varepsilon}_{mnk_{\mathrm{BC,BV}}}$). The density of electrons and holes per unit volume in the WL is given by

$$n, p_{\mathrm{WL}} = \frac{m^*_{e,h_{\mathrm{WL}}} KT}{2\pi\hbar^2 d_{\mathrm{WL}}} \cdot \log\left(1 + e^{\frac{E_{Fe,h} - E_{\mathrm{WL}_{\mathrm{CB,VB}}}}{KT}}\right)$$

where $m^*_{e,h_{\mathrm{WL}}}$ is the electron/hole effective mass in the WL and $E_{\mathrm{WL}_{\mathrm{CB,VB}}}$ is the CB/VB confined state energy in the WL.

III. NUMERICAL RESULTS

The model presented above can be applied to the analysis of the emission characteristics of zero-dimensional active materials with inhomogeneous broadening due to wide size fluctuations.

Since some experimental data (gain and ASE spectra) relative to the InAs–InP QDash-SOA presented in [35] were available to us, here we present the simulations that have led to the fitting of the measured data. These simulations have been performed to validate our model through a comparison with the experimental data and to estimate those material parameters that could not be obtained from measurements. At the end of this section, as an example of application of our model, we will discuss the effect of the average dash size and its fluctuations on the gain spectra.

The QDash SOA under investigation has a ridge waveguide structure that is 2.5-μm wide and 2.1-mm long. The SOA is based on a separate-confinement heterostructure with an active region comprising four InAs QDash layers, each separated by an InAlGaAs barrier 25-nm thick [8]. Since the separation among adjacent QDash layers is about ten times the QDash thickness, there is no vertical coupling among dashes.

From TEM analysis, the average dash transversal dimensions are known with a certain accuracy, whereas the longitudinal dimension is more questionable and in any case the spreading is rather significant. To gain experience in the fitting, we examined first the effect on the gain spectrum of the spreading in dash length. In Fig. 5, we analyze the effect of the length fluctuations with a dash cross section fixed to 17.3 nm × 1.9 nm. We plot the probability functions $P_{mnk}(\varepsilon)d\varepsilon$ in Fig. 5(a) and the corresponding material gain at various population inversions in Fig. 5(b). The QDdash ensemble has an average length of $\mu_L = 100$ nm and a Gaussian distributed length spreading with $\sigma_L = 20$ nm. In this simulation, only the $00k$ contributions were considered, because in the measured ASE (see Fig. 6) no clear secondary emission peaks due to first order transversal levels ($01k$) were observed. We found that this is due to the lateral [x direction in Fig. 1(a)] quantum mechanical coupling among dashes that causes the loss of confinement for the $01k$ states, whose wave functions are weakly confined in the uncoupled dash.

Fig. 5(a) (representing the probability functions $P_{mnk}(\varepsilon)d\varepsilon$) shows that the inhomogeneous broadening distributions caused
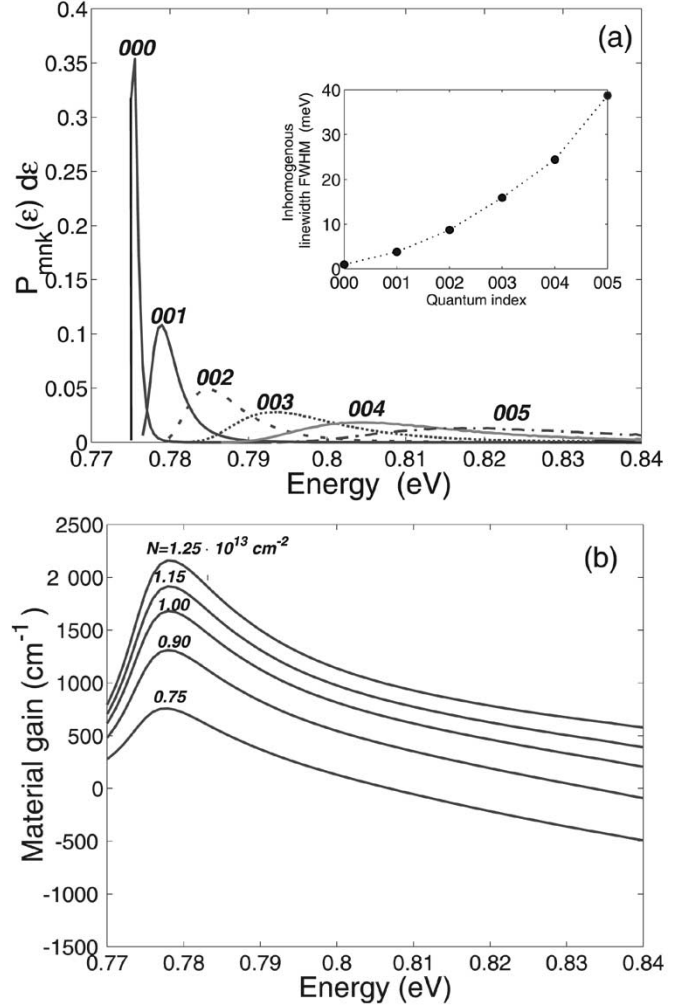

Fig. 5. (a) Probability functions $P_{mnk}(\varepsilon)d\varepsilon$ and, in the inset, the corresponding FWHM versus the longitudinal quantum index. (b) Resulting material gain increasing population inversion of an InAs–InP QDash ensemble with length fluctuations ($\mu_L = 100$ nm and $\sigma_L = 20$ nm) and cross section fixed to 17.3 nm × 1.9 nm.
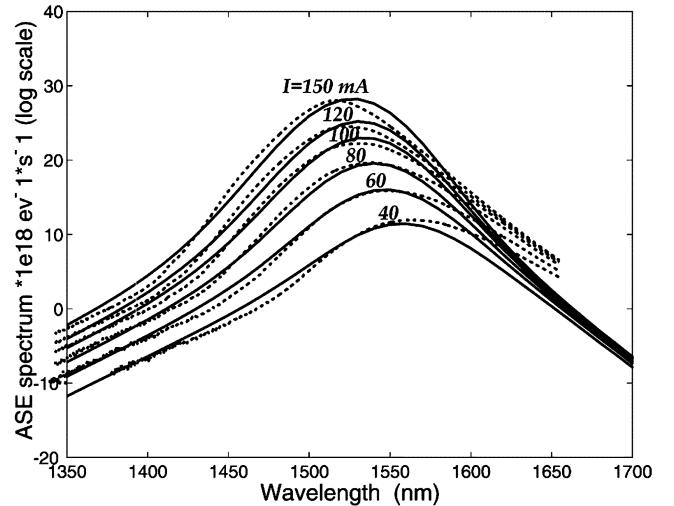

Fig. 6. Comparison between simulated (solid line) and measured (dotted line) ASE spectra of the InAs–InP SOA presented in [35].

by length fluctuations are strongly asymmetric around their peak value and therefore they cannot be fit with a Gaussian

or a Lorentzian shape. Furthermore, the width of the in-homogeneous broadening is significantly dependent on the recombination quantum index and its FWHM increases with k [see the inset of Fig. 5(a)].

We observe in Fig. 5(b) that high gain values are obtained only in a narrow energy range (between 0.77–0.79 meV, which is about a 40-nm wavelength span) and that the energy position of the gain peaks is independent of injected carriers. We also verified that the peaks do not shift varying the length spreading and their maximum value is only slightly dependent on σ_L. This happens because, for the transitions that mainly contribute to the gain spectrum (quantum index 000, 001, and 002), the width of the inhomogeneous broadening [see the inset of Fig. 5(a)] is narrower than or comparable to the homogeneous broadening bandwidth (10 meV FWHM). Therefore, the bandwidth of the emission spectrum is mainly due to the homogeneous broad-ening, and the length fluctuation has negligible effects. This is true also for any value of thickness and width spreading.

Running several other simulations with reduced dash length, we also found that for shorter dashes (i.e., $\mu_L < 40$ nm) length fluctuations are no longer negligible and such length variations have significant effects on the emission bandwidth and on the shape of the gain spectrum.

The gain spectra in Fig. 5(b) do not meet the typical behavior of the QDash system under investigation [35], characterized in-stead by a wide gain bandwidth. As a consequence, we suppose that the QDash ensemble we examine is mainly characterized by fluctuations in the size of the cross section, whereas the length fluctuations have a less significant effect on determining the width of the emission spectrum.

In order to quantify the effect of the cross-section-size fluctu-ations, we tried to fit the measured ASE spectra that were avail-able at different current injections (see Fig. 6). We have run sev-eral simulations considering various QDash ensembles, charac-terized by different average sizes and various spreadings of the transversal dimensions.

The simulated ASE spectra have been obtained from (3) and (4) according to

$$P_{ase}(\hbar\omega) = N_L w_{SOA} R_{spon}(\hbar\omega) \cdot \frac{e^{g_{net}(\hbar\omega)L_{SOA}} - 1}{g_{net}(\hbar\omega)} \quad (7)$$

where N_L is the number of QDash layers, w_{SOA} and L_{SOA} are the width and length of the SOA active region, $g_{net}(\hbar\omega) = \Gamma g_{mat}(\hbar\omega) - \alpha$ is the net modal gain, and α is the internal modal loss. Γ represents the optical field confinement factor in the dash active region and it is given by the product of the filling factor Γ_{xz} with the confinement factor Γ_y in the growth direction [19].

The best fitting results we obtained are shown in Fig. 6, where the simulated and measured ASE spectra are compared. To fit the measured data, it was important to introduce the effect of the strain. In our particle-in-a-box model, the strain has been taken into account as a modification of the InAs effective masses and of the energy gap with respect to the bulk case [24]. In partic-ular, we set an increased effective mass for the electrons ($m_e^* = 0.04m_0$, [25]) and we introduced effective masses dependent on direction ($m_{hh,\parallel}^* = 0.042m_0$ and $m_{hh,\perp} = 0.538m_0$ [25]) for the holes. Since in [2] an energy gap increase was calculated for

TABLE I
QDASH ENSEMBLE MATERIAL AND GEOMETRICAL PARAMETERS

Material Parameters

InAlGaAs/InP barrier

m_e^*	$0.059 \cdot m_0$, [36]
m_h^*	$0.43 \cdot m_0$, [36]
E_g	1.052 eV, [36]
CB offset	65.8% ΔE_g, [37]
VB offset	34.2% ΔE_g, [37]

InAs

m_e^*	$0.04 \cdot m_0$, [25]
$m_{hh,\parallel}^*$	$0.042 \cdot m_0$, [25]
$m_{hh,\perp}^*$	$0.538 \cdot m_0$, [25]
n_r	3.5
$2\Delta\gamma$	10 meV [21]

Ensemble Parameters

average length μ_L	180 nm
average thickness μ_h	2.1 nm
thickness fluctuation σ_h	0.28 nm
average width μ_w	15 nm
width fluctuation σ_w	0.8 nm
dash density N_s	$2.35 \cdot 10^{10}$ cm^{-2}
filling factor Γ_{xz}	63.45%
confinement factor Γ_y	1%
internal modal loss α	7 cm^{-1}
number of layers N_L	4

InAs-GaAs QD with strain, we have slightly increased the bulk InAs energy gap to match the simulated emission wavelength range with the measured one.

All parameters used in the simulation are listed in Table I for the InAs dash ensemble and InAlGaAs barrier. The table shows that the best fitting is obtained with an average length-to-width ratio of 12:1 and by introducing fluctuations in the QDash thick-ness and width. The length fluctuations were neglected because for long dashes, as in this case, the length spreading has a less significant effect on determining the gain bandwidth. We also observed that, with this set of parameters, the thickness fluctu-ations have a stronger effect on determining the emission band-width, whereas the width variation plays a less significant role. This is also in agreement with the results reported in [17] for InAs QD.
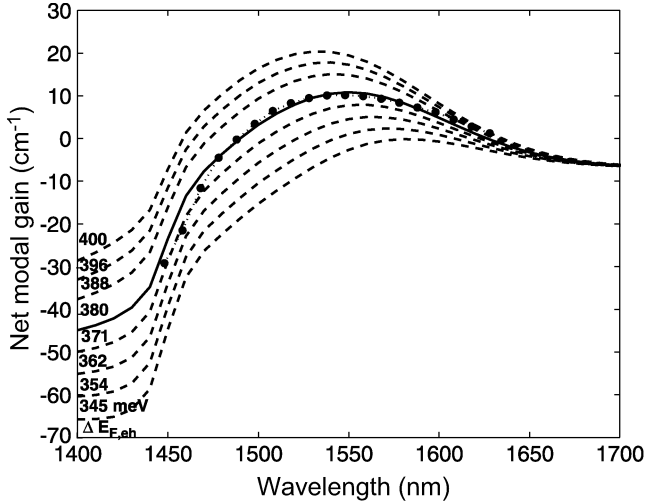
Fig. 7. Comparison between simulated (solid line) and measured (circles) net modal gain versus wavelength at 1.2 kA/cm^2. The net modal gain spectra simulated increasing the quasi-Fermi level separation ($\Delta E_{F,eh}$) are also shown as the dashed line.

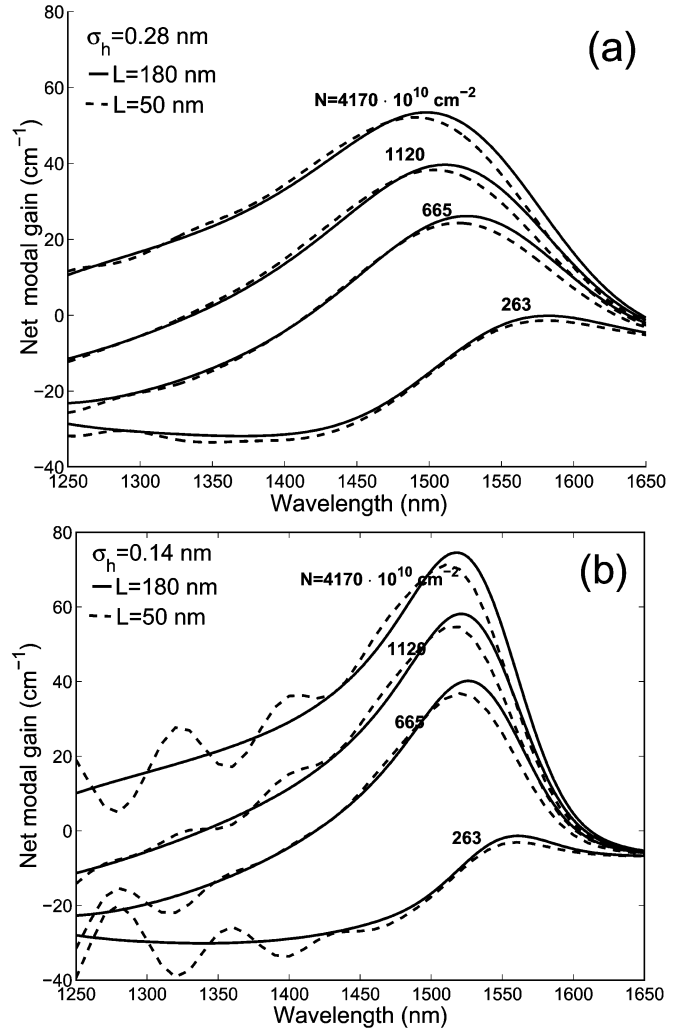

Fig. 8. Optical gain spectra at various carrier injections of two different dash ensembles characterized by short ($L = 50$ nm, dashed line) and long ($L = 180$ nm, solid line) dashes and thickness spreading of (a) $\sigma_h = 0.28$ nm and (b) $\sigma_h = 0.14$ nm around the average value of 2.1 nm.

With the obtained fitting parameters, the net modal gain has been calculated versus wavelength at increasing population inversion. The simulated results are shown in Fig. 7 and compared with the available measured curves of gain at 1.2 kA/cm^2 current injection.

From these simulations, we have found that, in order to match the ASE and the gain bandwidth, it was essential to introduce the thickness spreading. Indeed, as the thickness is the smallest QDash dimension (average width-to-thickness ratio about 7:1), even small thickness variations produce wide confined-state energy fluctuations, if compared to the energy level dispersion caused by the length and width spreading. Therefore, in this considered case, it is the thickness inhomogeneity that assures the wide emission bandwidth of the QDash material, whereas the long dash length guarantees adequate gain values for practical applications, thanks to the contribution of the several sufficiently filled longitudinal states ($00k$).

From these results, we demonstrate that, starting from a relatively well known set of parameters, we were able to fit with a good quantitative agreement the ASE and gain spectra. This validation of the proposed model allows the use of our code to predict and compare the gain characteristics of various ensembles with different average dash sizes and different size spreadings.

As an example, we compare in Fig. 8 the gain spectra of two QDash systems with two different dash lengths (50 and 180 nm), and we discuss the effect of thickness fluctuation in the two cases. The 50-nm value gives a length-to-width ratio of about 3:1 that corresponds to the minimum ratio for having a QDash behavior [11]. The comparison is done assuming that the two ensembles have the same spreading of the dash thickness and width and the same transversal and longitudinal separation (5 and 8 nm, respectively) among dashes. Therefore, the shorter dash ensemble has a higher density of dash per unit area (i.e., for $L = 50$ nm, $N_s = 7.9 \cdot 10^{10}$ cm^2, and $\Gamma_{xz} = 59.3\%$) compared to the longer dash ensemble (i.e., for $L = 180$ nm, $N_s = 2.35 \cdot 10^{10}$ cm^2, and $\Gamma_{xz} = 63.4\%$). This criterion was chosen because the gain spectra of the two ensembles, calculated at the same carrier injection per unit area ($N = N_s \cdot n_{\mathrm{QD}} + d_{\mathrm{WL}} \cdot n_{\mathrm{WL}}$),

have comparable gain. Fig. 8(a) shows that in the case of thickness spreading $\sigma_h = 0.28$ nm the two ensembles give very similar gain spectra for any carrier injection. We have also observed that this behavior maintains for any average dash length longer then 50 nm. On the contrary, in the case of a reduced thickness spreading ($\sigma_h = 0.14$ nm), the shape of the gain spectra depends more on the average dash length as shown in Fig. 8(b). For $L = 50$ nm, the secondary peaks due to higher order longitudinally confined states (003 at 1400 nm and 004 at 1320 nm) are clearly visible, whereas they are smoothed out in the spectrum of the $L = 180$ nm ensemble. We thus conclude that in the case of $\sigma_h = 0.28$ nm the QDash system shows a quantum-wire-like behavior [35], because the resulting emission characteristics are independent of the dash length. For $\sigma_h = 0.14$ nm, the effect of the longitudinal confinement is evident only in short dashes ($L = 50$ nm), whereas it disappears with longer dashes.

IV. CONCLUSION

In this paper, we have presented a numerical model that allows us to calculate the spectral emission characteristics (ASE

and gain) of a QDash active material. Starting from good estimates of the dash geometry and material composition and taking into account the effect of strain as a modification of the carrier effective masses compared to the bulk values, we were able to fit, with a good quantitative agreement, our simulated results with the measured ASE and gain spectra of an InAs–InP QDash SOA. We have found that the wide gain bandwidth of this investigated device is mainly determined by the thickness spreading (QDash smallest dimension) and secondarily by the presence of several confined states given by the dash elongated form. Our code has been used to predict the spectral emission characteristics of various QDash ensembles. In this paper, as an application example, the model has been used to evaluate the effect of the thickness fluctuations on the spectral emission characteristics of two different QDash ensembles characterized by long and short average dash lengths, respectively. The comparison has shown that in the case of wide dash thickness fluctuations (about 10% the average thickness) the gain spectra results are independent of the dash length, and the system presents a quantum-wire-like behavior. On the contrary, decreasing the thickness spreading to about 5% of the average thickness, the effects due to the longitudinal confinement appear only in the gain spectra of the short-dash ensemble.

ACKNOWLEDGMENT

REFERENCES

[1] M. Grundmann, *Nano-Optoelectronics*. Berlin, Germany: Springer-Verlag, 2002.

[2] H. Jiang and J. Singh, "Self-assembled semiconductor structures: electronic and optoelectronic properties," *IEEE J. Quantum Electron.*, vol. 34, pp. 1188–1196, July 1998.

[3] N. N. Lendestov, M. Grundman, F. Heinrichsdorff, D. Bimberg, V. M. Ustinov, A. E. Zhukov, M. V. Maximiv, Z. I. Alferov, and J. A. Lott, "Quantum-dot heterostructure lasers," *IEEE J. Select. Topics Quantum Electron.*, vol. 6, pp. 439–451, May/June 2000.

[4] M. Sugawara, K. Mukai, Y. Nakata, K. Otsubo, and H. Ishilkawa, "Performance and physics of quantum dot lasers with self-assembled columnar-shape and 1.3 μm emitting InGaAs quantum dots," *IEEE J. Select. Topics Quantum Electron.*, vol. 6, pp. 462–474, May/June 2000.

[5] S. Ghosh, P. Pradhan, and P. Bhatacharya, "Dynamic characteristics of high-speed $In_{0.4}Ga_{0.6}As/GaAs$ self-organized quatum dot lasers at room temperature," *Appl. Phys. Lett.*, vol. 81, no. 16, pp. 3055–3057, Oct. 2002.

[6] G. T. Liu, H. Li, A. Stintz, T. C. Newell, L. F. Lester, and K. J. Malloy, "Modal gain and T0 value improvements in quantum dot lasers using dots-in-a-well (DWELL) structure," in *Conf. Dig. IEEE 17th Int. Semiconductor Laser Conf.*, Sept. 25–28, 2000, pp. 133–136.

[7] R. H. Wang, A. Stintz, P. Varangis, T. Newell, H. Li, K. J. Malloy, and L. F. Lester, "Room-temperature operation of InAs quantum dash lasers on InP (001)," *IEEE Photon. Technol. Lett.*, vol. 13, pp. 767–769, Aug. 2001.

[8] R. Schwertberger, D. Gold, J. P. Reithmaier, and A. Forchel, "Long-wavelength InP-based quantum dash lasers," *IEEE Photon. Technol. Lett.*, vol. 14, pp. 735–737, June 2002.

[9] H. Htoon, J. Hollingworth, A. Malko, R. Dickerson, and V. Klimov, "Light amplification in semiconductor nanocrystals: quantum rods versus quantum dots," *Appl. Phys. Lett.*, vol. 82, no. 26, pp. 4776–4778, June 2003.

[10] L. F. Lester, A. Stintz, H. Li, T. C. Newell, E. A. Pease, B. A. Fuchs, and K. J. Malloy, "Optical properties of 1.24 μm quantum dot lasers," *IEEE Photon. Technol. Lett.*, vol. 11, pp. 931–933, 1999.

[11] A. Stintz, P. Varangis, K. Malloy, L. Lester, T. Newell, and H. Li, "Quantum Dash Devices," U.S. Patent 6 600 169, July 29, 2003.

[12] J. P. Reithmaier, L. Bach, W. Kaiser, R. Schwetberger, A. Forchel, A. Bilenca, R. Alizon, V. Mikhelashvili, D. Dahan, and G. Eisenstein, "InAs on InP quantum dots for optoelectronic applications," in *Proc. Eur. Conf. Lasers and Electro-Optics (CLEO/EUROPE)*, Munich, Germany, June 2003.

[13] A. Bilenca, R. Alizon, V. Mikhelashvili, G. Eisenstein, R. Schwertberger, D. Gold, J. P. Reithmaier, and A. Forchel, "InAs/InP 1550 nm quantum dash semiconductor optical amplifiers," *Electron. Lett.*, vol. 38, no. 22, pp. 1350–1351, Oct. 2002.

[14] L. Bach, W. Kaiser, R. Schwertberger, J. P. Reithmaier, and A. Forchel, "1.54 m single mode InP-based Q-dash lasers," *Electron. Lett.*, to be published.

[15] H. Li, T. Liu, P. M. Varangis, T. C. Newell, A. Stintz, B. Fuchs, K. J. Malloy, and L. F. Lester, "150-nm tuning range in a grating-coupled external cavity quantum dot laser," *IEEE Photon. Technol. Lett.*, vol. 12, pp. 759–761, July 2000.

[16] D. Pal, V. G. Stoleru, E. Towe, and D. Firsov, "Quantum dot size variation and its impact on emission and absorption characteristics: an experimental and theoretical modeling investigation," *Jpn. J. Appl. Phys.*, vol. 41, no. 2A, pp. 482–489, Feb. 2002.

[17] A. Endoh, Y. Nakata, Y. Sugiyama, M. Takatsu, and N. Yokoyama, "Effect of size fluctuations on the photoluminescence spectral linewidth of closely stacked InAs self-assembled quantum dot structures," *Jpn. J. Appl. Phys.*, vol. 38, no. 2B, pp. 1085–1089.

[18] O. Qasaimeh, "Effect of inhomogeneous line broadening on gain and differential gain of quantum dot lasers," *IEEE Tran. Electron Devices*, vol. 50, pp. 1575–1581, July 2003.

[19] L. V. Asryan and R. A. Suris, "Inhomogeneous line broadening and the threshold current density of a semiconductor quantum dot laser," *Semicond. Sci. Technol.*, vol. 11, pp. 554–567, 1996.

[20] R. Alizon, A. Bilenca, H. Dery, V. Mikhelashvili, G. Eisenstein, R. Schwertberger, D. Gold, J. P. Reithmaier, and A. Forchel, "Cross gain modulation in inhomogeneously broadened gain spectra of InP based-1550 nm quantum-dash optical amplifiers: small signal bandwidth dependence on wavelength detuning," *Appl. Phys. Lett.*, vol. 82, no. 26, pp. 4660–4662, June 2003.

[21] M. Sugawara, K. Mukai, Y. Nakata, and H. Ishikawa, "Effect of homogeneous broadening of optical gain on lasing spectra in self-assembled $In_XGa_{1-X}As/GaAs$ quatum dot lasers," *Phys. Rev. B*, vol. 61, pp. 7595–7603, Mar. 2000.

[22] M. Sugawara, K. Mukai, and Y. Nakata, "Light emission spectra of columnar-shaped self-assembled InGaAs/GaAs quantum-dot lasers: effect of homogeneous broadening of the optical gain on lasing characteristics," *Appl. Phys. Lett.*, vol. 74, pp. 1561–1563, Mar. 1999.

[23] D. G. Deppe, H. Huang, and O. B. Shchekin, "Modulation characteristics of quantum-dot lasers: the influence of p-type doping and the electronic density of states on obtaining high speed," *IEEE J. Quantum Electron.*, vol. 38, pp. 1587–1593, Dec. 2002.

[24] D. Bimberg, M. Grundmann, and N. N. Ledenstov, *Quantum Dot Heterostructures*. Chichester, U.K.: Wiley, 1999.

[25] L. W. Wang, A. J. Williamson, A. Zunger, H. Jiang, and J. Singh, "Comparison of k · p and direct diagonalization approaches to the electronic structure of InAs/GaAs quantum dots," *Appl. Phys. Lett.*, vol. 76, no. 3, pp. 339–341, Jan. 2000.

[26] M. Grundmann, O. Stier, and D. Bimberg, "InAs/GaAs pyramidal quantum dots: strain distribution, optical photons and electronic structure," *Phys. Rev. B*, vol. 52, no. 16, pp. 11 969–11 981, Oct. 1995.

[27] M. Asada, Y. Miyamoto, and Y. Suematsu, "Gain and threshold of three-dimensional quantum-box lasers," *IEEE J. Quantum Electron.*, vol. QE-22, pp. 1915–1921, Sept. 1986.

[28] P. S. Zory, *Quantum Well Lasers*. San Diego, CA: Academic, 1993.

[29] M. Sugawara, *Self-Assembled InGaAs/GaAs Quantum Dots*. New York: Academic, 1999.

[30] Y. Suematsu and A. R. Adams, *Handbook of Semiconductor Lasers and Photonic Integrates Circuits*. London, U.K.: Chapman and Hall, 1994.

[31] M. Abramowitz and I. Stegun, *Handbook of Mathematical Functions*. New York: Dover, 1972.

[32] D. G. Deppe, D. L. Huffaker, S. Csutak, Z. Zou, G. Park, and O. B. Shchekin, "Spontaneous emission and threshold characteristics of 1.3 μm InGaAs-GaAs quantum dot GaAs-based laser," *IEEE J. Quantum Electron.*, vol. 35, pp. 1238–1246, Aug. 1999.

[33] H. Huang and D. G. Deppe, "Rate equation model for nonequilibrium operating conditions in a self-organized quantum-dot laser," *IEEE J. Quantum Electron.*, vol. 37, pp. 691–698, May 2001.

[34] H. Jiang and J. Singh, "Nonequilibrium distribution in quantum dots lasers and influence on laser spectral output," *J. Appl. Phys.*, vol. 85, no. 10, pp. 7438–7442, May 1999.

[35] H. Dery, E. Benisty, A. Epstein, R. Alizon, V. Mikhelashvili, G. Eisenstein, R. Schwertberger, D. Gold, J. P. Reithmaier, and A. Forchel, "On the nature of InAs/InP quantum dash gain media," in *Proc. Eur. Conf. Optical Commununications*, Rimini, Italy, Sept. 2003, paper We2.5.4.

[36] S. L. Chuang, *Physics of Optoelectronic Devices*. New York: Wiley Interscience, 1995.

[37] T. Ishikawa and J. E. Bowers, "Band lineup and in-plane effective mass of InGaAsP or InGaAlAs on InP strained-layer quantum well," *IEEE J. Quantum Electron.*, vol. 30, pp. 562–570, Feb. 1994.

Mariangela Gioannini was born in Cuorgnè, Italy, in 1973. She received the M.S. degree in electronic engineering and the Ph.D. degree in electronic and communication engineering from Politecnico di Torino, Torino, Italy in 1998 and 2002, respectively.

She currently holds a postdoctoral position with Dipartimento di Electronica, Politecnico di Torino. Her research interests include modeling, design, and characterization of multisection semiconductor lasers and theoretical investigation of semiconductor quantum dot and quantum dash materials for lasers and optical amplifiers.